Band Offsets and Contacts in Monolayer Black Phosphorus

Yuzheng Guo[1]*, and John Robertson[2]

1 College of Engineering, Swansea University, Swansea, SA1 8EN

2 Engineering Department, Cambridge University, Cambridge, CB2 1PZ, UK

E-mail address of corresponding author: yuzheng.guo@swansea.ac.uk

Abstract: Black phosphorus is a new member of 2D materials for field effect transistor application due to its atomic monolayer structure and high electron and hole mobility. The FET application requires the knowledge of b-P interface with high-k oxide and metal electrodes. In this work the band offsets for gate insulators such as HfO_2 on black phosphorus (b-P) are calculated using density functional theory. It is confirmed that HfO_2 can provide good band alignment for both conduction and valence band. The Schottky barrier heights are also calculated for the monolayer and bulk using the supercell model, for the perfect interface with no defects in the b-P. A strong p-type Fermi level pinning has been observed due to stronger metal-P bonding.

1. Introduction

The 2D materials have received a lot of attention since the discovery of graphene[1]. However, there is no simple way to open up a band gap without significantly lowering its performance. The discovery of first semiconducting 2D materials, the transition metal dichalcogenides (TMDs) like MoS_2, opens up the way to fabricate field effect transistors with atomically thin materials[2-4]. However, the carrier mobility in the TMDs is limited by their d-like band edge character[4,5]. The semi-local d electrons contribute much to both the valence band and conduction band edges so both the electron and hole mobilities in all TMDs are affected. The strong Fermi level pinning and intrinsic defects in TMD also hinders further application in FET[6-9]. Therefore, people are still searching for different semiconducting 2D materials with higher mobility.

Recently the black phosphorus (b-P) based devices has been fabricated [10-25]. The black phosphorous has a buckled layer structure with 3-fold covalent bonding within each layer and van der Waals bonding between each layer. Each monolayer has top and bottom P atoms labelled as light and dark atoms in Figure 1(a). Compared to graphene, the lower symmetry gives b-P a band gap. There is a direct band gap in few-layer. The monolayer has a direct band gap of 1.5eV while the bulk band gap is about 0.3eV [10,11]. Its band edges are purely p-type so the carrier mobility is much higher than those of MoS_2 because p states are less sensitive to disorder and localisation than d states [12-13]. Field effect mobilities as high as 1000-2000 $cm^2V^{-1}s^{-1}$ have been reported by various experimental groups [10-14]. Theoretical predictions of upper limit is 10,000 $cm^2\ V^{-1}\ s^{-1}$[15-18]. In our previous work we have discussed the intrinsic defects and possible doping strategies of monolayer black phosphorous and other TMDs[25-28]. However, the interface between 2D materials and electrodes/gate oxide is also critical in FET applications.

In this work, we further examine the band alignment of b-P with other oxides and 2D materials for hetrostructure application such as tunnel FET and defect-free interfaces

between b-P and several metals. It is found that HfO_2 is a good high-k oxide for both monolayer and bulk b-P. Just like the TMD monolayers, there is strong p-type Fermi level pinning for both monolayer and bulk b-P. The pinning factor is calculated to be 0.11 for monolayer and 0.10 for bulk. This indicates that it is even more difficulty to control the Schottky barrier height by electrode in b-P than in TMDs.

2. Methods

The simulations were carried out using the plane-wave pseudo potential code CASTEP [29]. The GGA suffers from the well-known band gap error and thus cannot give correct band alignment for semiconductors and insulators. Critically, GGA gives a negative band gap for bulk b-P. The screened exchange (SX) hybrid functional is known to be able to correct the band error in both bulk and 2D materials [26, 27]. SX is applied in the calculation of band offsets of various 2D materials. The same pseudopotentials and parameters are used as in our previous works in 2D materials. The band gap of few layer and bulk b-P is shown in Figure 2(b), consistent with experimental values and other simulations. The hybrid functional is too resource consuming for large supercell of metal:b-P models. Therefore, the PBE-style generalized gradient approximation (GGA) is used for geometry relaxation of the stack models and Schottky barrier height calculation in this paper.

A 6-layer b-P is used to represent bulk b-P during the SBH calculation. The supercell lattice is set to the lattice constant of b-P and the strain is applied purely in metal part. The b-P primitive cell is first relaxed to compare the lattice constant with experimental values, as shown in Table 1. The difference is less than 2%. A 5x5 or 4x4 b-P supercell is used for the interface model. The strain is below 5% in all our models. For k sampling, we took the Γ point scheme for the defect model due to the large supercell. The cut off energy of 480eV is chosen in all GGA based calculations. For the electrodes, we use the metals Sc, Al, Cr, Ru, Co, Ni, Pd, Pt, to cover a wide range of work functions to test the Fermi level pinning. The (0001) surface is used for hexagonal close packed (HCP) metals and (100) surface is used for face centred cubic (FCC) metals when constructing the supercells. The atomic structures for HCP and FCC structure metal/b-P used in this work are shown in Figure 2 for Sc and Pt respectively. The work function ranges from 3.5eV (Sc) to 5.65eV (Pt). The experimental work functions are taken from Michaelson [58]. The strong van der Waals interaction has been confirmed in many 2D materials. In our simulation, the TS scheme is used to include van der Waals correction empirically in all the supercell calculation with a metal:b-P interface.

The charge neutrality level can be calculated from the density of states N(E), as shown in Figure 1 (c), as the energy at which the Greens function is zero,

$$G(E) = \int \frac{N(E').dE'}{E - E'} = 0 \qquad (1)$$

All the DOS enters this equation. This gives a CNL energy of 0.36 eV above the valence band in the monolayer.

The SBHs are extracted as the energy difference from the top of the valence band to the metal Fermi energy. The valence band top is difficult to identify in the supercell density of states or surface band structure. So we use instead the theoretical analogue of the Kraut's photoemission method [60] and use the P 3s core level as a reference level to compare the valence band top in the isolated case to the metal supercell case. The s orbital is 13-15eV below the Fermi level, deep in the valence band.

3. Results

Figure 3 shows the band alignment of monolayer b-P and bulk b-P with HfO_2. The band offsets between both b-P for conduction band and valence band is larger than 1eV. Therefore HfO2 is a good candidate as high-k oxide for few-layer b-P.

Another important strategy for band engineering in 2D materials is by stacking different layers of 2D materials together. The van der Waals gap between different materials can provide an atomically sharp interface if no defect and doping presented in the monolayer. Many important applications requires specific band alignment between the monolayers. In figure 2 we also show the band alignment of b-P with other 2D materials including TMDs and III-IV monolayers. Tunnel FET requires a type III hetrostructure. It is obvious that bulk b-P provide the highest VBM and lowest CBM in all the materials. Therefore it is a good candidate for both valence band and conduction band part in a TFET. Therefore WSe2/b-P or b-P/HfS2 are two potential pairs for TFET. The different symmetry of b-P and other 2D materials could effectively minimize the interaction between the two parts, which could further lower the sub-threshold leakage.

Contact resistance limits device performance for many 2D semiconductors. Hence we have calculated the band alignments of metals on b-P for the top contact geometry, for the case of ideal contacts (no defects, phosphorus vacancies). The calculated p-type barrier heights are shown in Fig 6 for a wide range of metals plotted against the metal work function. The pinning factor S (slope of this plot) is found to be 0.1 for the bulk and S=0.11 for the monolayer. This is strong pinning. The pinning factor for TMDs is usually from 0.2-0.3. The pinned Fermi level is close to valence band due to the charge neutrality level (also plotted in the figure) being close to valence band. The strong pinning occurs because the metal atoms become quite close to the P atoms, as shown in Fig 4, and thus form chemical bonds. The distance is smaller than that of MoS2 interface. It is not van der Waals bonding as it is between metal atoms and carbon as at graphene contacts. This is due to the lone pair of P atom forming bonds to the metal interface. The exposed lone pair can interact with metal actively. The strong pinning is in the absence of defects. If intrinsic defect is presented such as P vacancy, the pinning factor should be even smaller. A similar strong bonding occurs for metals on MoS_2 [4]. Thus, we cannot change barrier heights much by varying the metal. Nevertheless, barrier heights are small or zero for p-type doping.

4. Conclusions

In summary, we calculated the band offsets and metal contact for monolayer and bulk b-P. HfO_2 is identified as a good high-k gate oxide for b-P. The band offsets between HfS2 and WSe2 with b-P allow possible high speed TFET based on these 2D materials. The metal contact shows a strong p-type Fermi level pinning with a pinning factor about 0.1, even smaller than that of TMDs. However, the p-type Schottky barrier heights are small or zero.

References

1. A K Geim, K S Novoselov, Nat. Mats. 6 183 (2007)
2. B Radisavljevic, A Radenovic, J Brivio, V Giacometti, A Kis, Nature Nano. 6 147 (2011)
3. G Fiori, F Bonaccorso, G Iannaccone, T Palacios, D Neumaier, A Seabaugh, S K Banerjee, L Colombo, Nat Nano 9 768 (2014)
4. M. S. Fuhrer, J. Hone, Nature Nano 8, 146 (2013)
5. R Fivaz, E Mooser, Phys Rev 163 743 (1967).
6. S. Das, H. Y. Chen, A. V. Penumatcha, J. Appenzeller, NanoLett 13 100 (2013)
7. S McDonnell, R Addou, C Buie, R M. Wallace, C L. Hinkle, ACS Nano 8, 2880 (2014)
8. S Chuang, C Battaglia, A Azcatl, S McDonnell, J S Kang, X Yin, M Tosun, R Kapadia, H Fang, R M Wallace, A Javey, Nanoletts 14 1337 (2014)
9. Y Guo, D Liu, J Robertson, submitted (2014)
10. L Li, Y Yu, Q Ge, X Ou, H Wu, D Feng, X H Chen, Y Zhang, Nature Nanotech. 9, 372 (2014)
11. H Liu, A T Neal, Z Zhu, X Xu, D Tomanek, P D Ye, ACS Nano 8 4033 (2014);
12. S. Koenig, R. Doganov, H. Schmidt, A. H Castro Neto, B. Ozyilmaz, Appl. Phys. Lett. 104, 103106 (2014)
13. J. Qiao, X. Kong, Z.-X. Hu, F. Yang, W. Ji, Nature Commun, 5, 4475 (2014)
14. A Morita, Appl Phys A 39227 (1986)
15. F. Xia, H. Wang, Y. Jia. Nature Commun, 5 4458 (2014)
16. Z. Zhu, D. Tomanek, Phys. Rev. Lett., 112, 176802 (2014)
17. A S. Rodin, A. Carvalho, A.H. Castro Neto, Phys. Rev. Lett. 112, 176801 (2014)
18. V. Tran, R. Soklaski, Y. Liang, L. Yang, Phys. Rev. B. 89 235319 2014）
19. R Fei, L Yang, Nano Lett. 14, 2884 (2014)
20. P Li, I Appelbaum, Phys Rev B 90 115439 (2014)
21. A N Rudenko, M I Katsnelson, Phys Rev B 89 201408 (2014)
22. Y.Cai, G. Zhang, Y.W. Zhang, Sci. Report 4,6677 (2014)
23. Y Liu, F Xu, Z Zhang, E S Penev, B I Yakobson, Nanolets 14 6782 (2014)
24. T Takahashi, H Tokailin, S Suzuki, T Sagawa, I Shirotani, Phys Rev B 29 1105 (1984); C Q Han et al, Phys Rev B 90 05101 (2014)
25. Y. Guo and J. Robertson, Sci Rep. 5 14165 (2015)
26. S. J. Clark and J. Robertson, Phys Rev B 82 085208 (2010).
27. D. Liu, Y. Guo, L. Fang, J. Robertson, Appl. Phys. Lett.103 183113 (2013)
28. Guo, Yuzheng; John, Robertson; ACS Applied Material & Interface, 7, 25709 (2015)
29. S. J. Clark, M. D. Segall, C. J. Pickard, P. J. Hasnip, M. J. Probert, K. Refson, and M. C. Payne, Kristallogr. 220, 567 (2005)
30. S. Grimme. J. Comp. Chem. 27, 1787 (2006)

		a	b	c
Bulk	Experiment [30]	10.47	3.31	4.37
	This work	10.794	3.291	4.379
Monolayer	Other work		3.32	4.58
	This work		3.279	4.521

Table 1 Calculated lattice constants for b-P.

Figure Captions:

Fig. 1 (a) Atomic structure of monolayer b-P. Light and dark colours are used distinguished between top and bottom layer P atoms. (b) Band gap of few layer b-P as a function of layer number. (c) The density of states for monolayer b-P.

Fig. 2 Atomic structure of Pt (a) and Sc (b) on top b-P. A supercell size of 2 and 7 is used for Pt and Sc respectively. Pt – dark blue. Sc – silver.

Fig. 3 Band alignment of various 2D materials and HfO_2.

Fig. 4 Fermi level pinning of metal contact on monolayer and bulk b-P. The VBM is set to be 0. CBM is labelled on top of the figure. The slope of the fitted line is extracted as pinning factor. CNL is also labelled for comparison.

Fig. 5 The bond length of P-metal bond formed in the interface.

Fig. 1

(a)

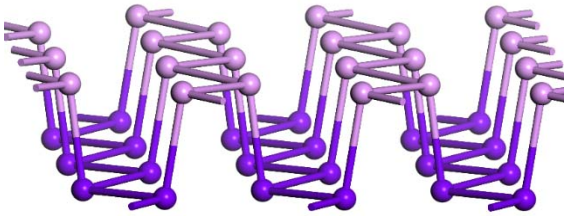

(b)

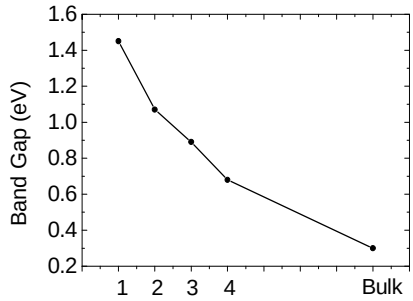
Band Gap (eV)
1.6
1.4
1.2
1.0
0.8
0.6
0.4
0.2
1
2
3
4
Bulk

(c)

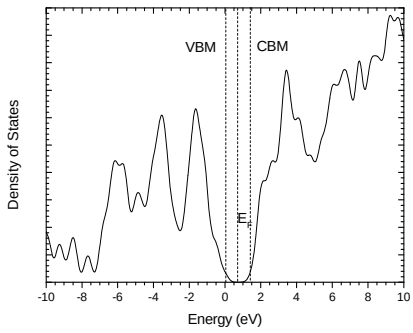
VBM
CBM
E_F
Density of States
-10
-8
-6
-4
-2
0
2
4
6
8
10
Energy (eV)

Fig. 2

(a)

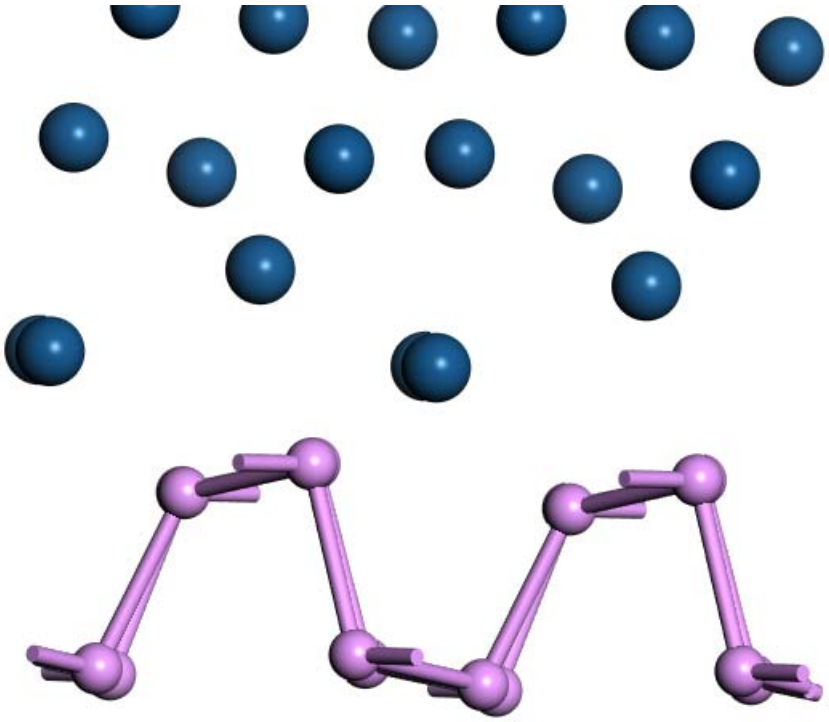

(b)

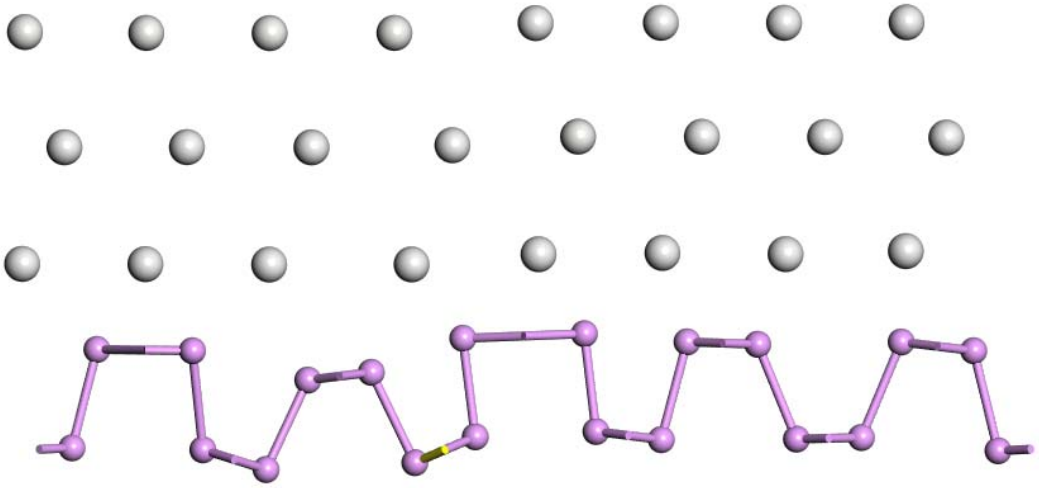

Fig. 3

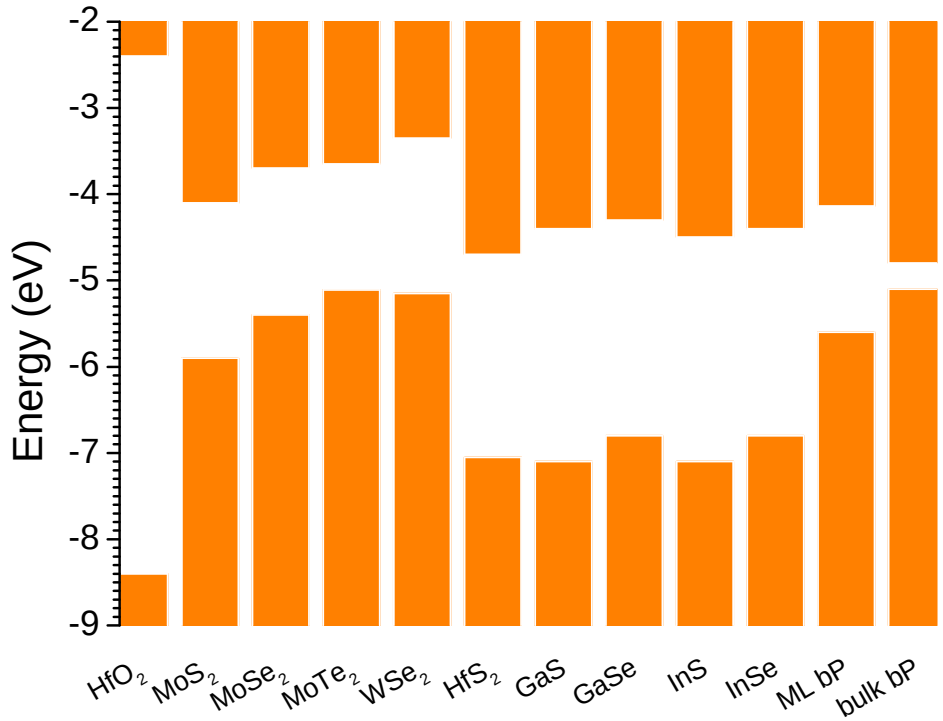
Energy (eV)
-2
-3
-4
-5
-6
-7
-8
-9
HfO2
MoS2
MoSe2
MoTe2
WSe2
HfS2
GaS
GaSe
InS
InSe
ML bP
bulk bP

Fig. 4

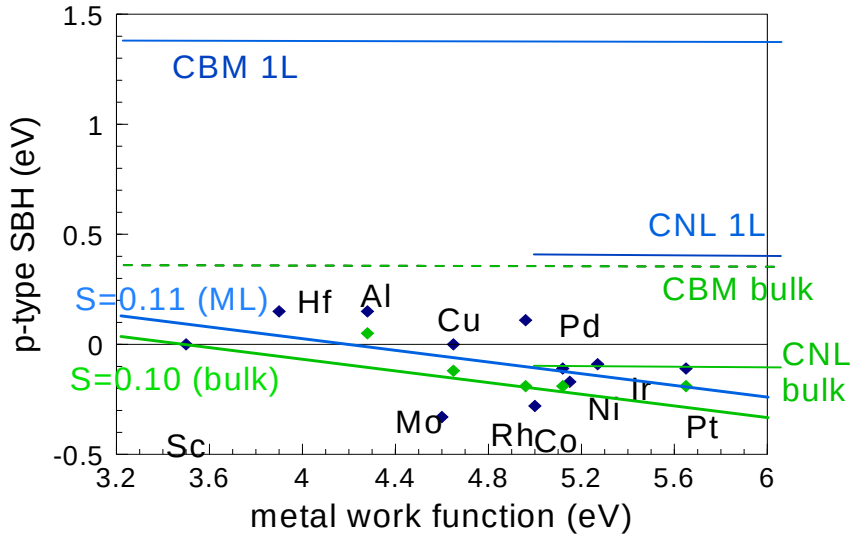
1.5
1
0.5
0
-0.5
p-type SBH (eV)
CBM 1L
CNL 1L
CBM bulk
CNL
bulk
S=0.11 (ML)
S=0.10 (bulk)
Hf
Al
Cu
Pd
Ir
Ni
Mo
Rh
Co
Pt
Sc
3.2
3.6
4
4.4
4.8
5.2
5.6
6
metal work function (eV)

Fig. 5

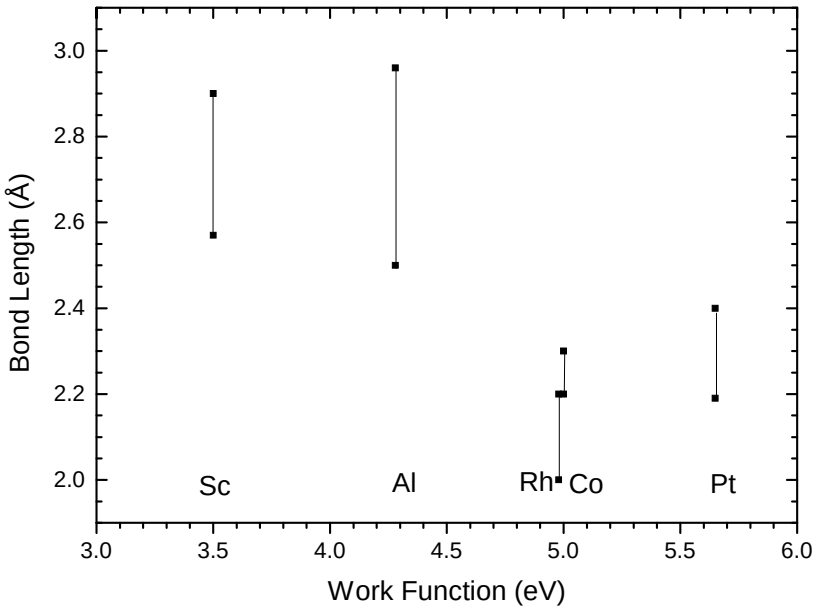
Bond Length (Å)
3.0
2.8
2.6
2.4
2.2
2.0
Sc
Al
Rh
Co
Pt
3.0
3.5
4.0
4.5
5.0
5.5
6.0
Work Function (eV)